

Exclusive J/ψ photo-production on nuclei

Sang-Ho Kim,^{1,*} T.-S. H. Lee,^{2,†} and R.B. Wiringa^{2,†}

¹*Department of Physics and Origin of Matter and Evolution of Galaxies (OMEG) Institute, Soongsil University, Seoul 06978, Korea*

²*Physics Division, Argonne National Laboratory, Argonne, Illinois 60439, USA*

(Dated: November 20, 2024)

Motivated by the recent experimental developments, the Pom-CQM model of the $\gamma+N \rightarrow J/\psi+N$ reaction of Lee *et al.* [Eur. Phys. J. A. **58**, 252 (2022)] and Sakinah *et al.* [Phys. Rev. C. **109**, 065204 (2024)] has been applied to predict the exclusive J/ψ photo-production on nuclei (A). Within the multiple scattering theory, the calculations have been performed by including the impulse amplitude $T_{J/\psi A, \gamma A}^{\text{IMP}}$ and the J/ψ -nucleus final state interaction (FSI) amplitude $T_{J/\psi A, \gamma A}^{\text{FSI}}$. For the deuteron target, $T_{J/\psi d, \gamma d}^{\text{IMP}}$ is calculated exactly using the wave function generated from the realistic nucleon-nucleon potentials. It is found that, near the threshold region, the J/ψ photo-production cross sections depend sensitively on the d -state of the deuteron wave function. The FSI amplitude $T_{J/\psi A, \gamma A}^{\text{FSI}}$ is calculated using the first-order optical potential constructed from the J/ψ - N scattering amplitude generated from the employed Pom-CQM model. It turns out that the FSI has significant effects in the large momentum-transfer region. By using the conventional fixed scatter approximation (FSA) and the nuclear form factors from the variational Monte-Carlo (VMC) calculations of Lonardoni *et al.* [Phys. Rev.C. **96**, 024326 (2017)], the cross sections of the J/ψ photo-production on ^4He , ^{16}O , and ^{40}Ca are also predicted for future experimental investigations at JLab and EIC.

I. INTRODUCTION

It is well recognized [1] that the study of J/ψ photo-production on the nucleon can be used to explore the role of gluons in determining the properties of the nucleon and hadron-hadron interactions. The experimental data of $\gamma + p \rightarrow J/\psi + p$ at photon energies near the threshold region ($8.90 \leq E_\gamma \leq 10.90$ GeV) have recently been reported by the Jefferson Laboratory (JLab) [2–4] and have been analyzed within several theoretical models [5–10] and also recently in Refs. [11, 12]. With the developing experimental and theoretical efforts, the data of J/ψ photo-production on nuclei will be also available at JLab [13–17] in the near future, and eventually at Electron-Ion Collider (EIC) [18–20].

The EIC has the capability to measure the diffractive and exclusive processes with a variety of ion beams and will provide the first 3-dimensional images of sea quarks and gluons in a fast-moving nucleus with sub-femtometer resolution. For example, the EIC can obtain the spatial distribution of gluons in a nucleus by measuring the coherent diffractive production of J/ψ in electron-nucleus scattering, as in the case of electron-proton scattering. Coherent exclusive processes, in which the nucleus stays intact, can give us valuable insights into understanding collective dynamics such as shadowing, anti-shadowing or the EMC effect [18].

The purpose of this work is to help facilitate these efforts by applying the Pom (Pomeron)-CQM (constituent quark model) model of the $\gamma + N \rightarrow J/\psi + N$ reaction

developed in Refs. [1, 11] to predict the cross sections of the exclusive J/ψ photo-production on nuclei (A) and to investigate how these cross sections are related to the nuclear structure, as a step to develop an approach to investigate the role of gluons in nuclei. We will perform the calculations within the well developed multiple scattering theory [21–25] and will present the predicted cross sections of the exclusive J/ψ photo-production on the deuteron (d), ^4He , ^{16}O , and ^{40}Ca targets. For $A > 2$ nuclei, we extend our previous work on $\gamma + ^4\text{He} \rightarrow \phi + ^4\text{He}$ [26] where the LEPS (Laser Electron Photon Experiment at SPring-8) data [27] are fairly accounted for. Previous theoretical studies on $\gamma + A \rightarrow J/\psi + A$ are very rare [28, 29]. We are also motivated by Ref. [28] to explore how the nuclear short range correlations can be probed by J/ψ photo-production reactions.

This paper is organized as follows. In Sec. II, we briefly review the Pom-CQM model constructed in Refs. [1, 11]. The formulation of J/ψ photo-production on nuclei is presented in Sec. III. The numerical results are presented in Sec. IV for the deuteron target and in Sec. V for the ^4He , ^{16}O , and ^{40}Ca targets. In Sec. VI, we summarize the present work and discuss possible improvements which are needed to investigate the roles of gluons in nuclei using the data from future experiments. In the Appendix, we provide the explanation for the Pom-CQM model which is used for the calculations in this work and is needed to develop the formulation of the J/ψ photo-production reactions on nuclei.

II. POM-CQM MODEL

With the normalization [30] $\langle \mathbf{k} | \mathbf{k}' \rangle = \delta(\mathbf{k} - \mathbf{k}')$ for plane wave state $|\mathbf{k}\rangle$ and $\langle \phi_\alpha | \phi_\beta \rangle = \delta_{\alpha, \beta}$ for bound state

* shkimphy@gmail.com

† tshlee@anl.gov

$|\phi_\alpha\rangle$, the differential cross section of the J/ψ (also denoted as V) photo-production reaction, in the center of mass (c.m.) frame, $\gamma(\mathbf{q}, \lambda) + N(-\mathbf{q}, m_s) \rightarrow V(\mathbf{k}, m_V) + N(-\mathbf{k}, m_{s'})$, is calculated from [1]

$$\frac{d\sigma_{VN,\gamma N}}{d\Omega} = \frac{(2\pi)^4 |\mathbf{k}| E_V(\mathbf{k}) E_N(\mathbf{k}) |\mathbf{q}|^2 E_N(\mathbf{q})}{|\mathbf{q}|^2 W W} \times \frac{1}{4} \sum_{m_{s'}, m_s} \sum_{m_V, \lambda} |\langle \mathbf{k}, m_V m_{s'} | T_{VN,\gamma N}(W) | \mathbf{q}, \lambda m_s \rangle|^2, \quad (1)$$

where m_a denotes the z -component of the spin of particle a , $E_\alpha(\mathbf{k}) = \sqrt{\mathbf{k}^2 + m_\alpha^2}$ is the energy of a particle α with mass m_α , and λ is the helicity of photon γ . The magnitudes $q = |\mathbf{q}|$ and $k = |\mathbf{k}|$ are defined by the invariant mass $W = q + E_N(q) = E_V(k) + E_N(k)$.

Within the Pom-CQM model [1, 11], the reaction amplitude $T_{VN,\gamma N}(W)$ can be expressed as the sum of the dynamical scattering amplitude $T_{VN,\gamma N}^D(W)$ and the Pomeron-exchange amplitude $T_{VN,\gamma N}^{\text{Pom}}(W)$

$$T_{VN,\gamma N}(W) = T_{VN,\gamma N}^D(W) + T_{VN,\gamma N}^{\text{Pom}}(W). \quad (2)$$

The amplitude $T_{VN,\gamma N}^D(W)$, defined within a Hamiltonian formulation [31–33], is of the following form

$$T_{VN,\gamma N}^D(W) = B_{VN,\gamma N}(W) + T_{VN,\gamma N}^{\text{FSI}}(W), \quad (3)$$

where $B_{VN,\gamma N}(W)$ is the amplitude of the photo-production of J/ψ on the nucleon and the final state interaction (FSI) amplitude is of the following form

$$T_{VN,\gamma N}^{\text{FSI}}(W) = t_{VN,VN}(W) \frac{1}{E - H_0 + i\epsilon} B_{VN,\gamma N}(W). \quad (4)$$

Here H_0 is the free Hamiltonian and $t_{VN,VN}(W)$ is the $J/\psi N \rightarrow J/\psi N$ scattering amplitude calculated from the $J/\psi N$ potential $v_{VN,VN}$ using the following Lippmann-Schwinger equation

$$t_{VN,VN}(W) = v_{VN,VN} + v_{VN,VN} \frac{1}{W - H_0 + i\epsilon} t_{VN,VN}(W). \quad (5)$$

Within QCD, the Born term $B_{VN,\gamma N}(W)$ and $v_{VN,VN}$ are defined by the interactions between quarks in the J/ψ and nucleon due to the gluon-exchange mechanisms. The formulation of $B_{VN,\gamma N}(W)$ and $v_{VN,VN}$ depends on the models of the J/ψ and N . The most straightforward approach is to use the CQM [34] within which both quantities are defined by the loop-integrations of gluon-exchange quark-quark potential v_{qq} over the wave function of J/ψ and N . This CQM-based model was first explored in Ref. [1] and developed in Ref. [11] to analyze the JLab data [2–4] using a simplification that the interactions are defined by the phenomenological quark- N potentials $v_{cN}(r)$. Thus $B_{VN,\gamma N}(W)$ and $v_{VN,VN}$ are calculated from one-loop integrations of $v_{cN}(r)$ over the J/ψ wave function, as shown in Figs. 1 and 2, respectively.

The fits to the JLab data are obtained by adjusting the parameters of the phenomenological quark- N potentials which are of the following forms

$$v_{cN}^B(r) = \alpha_B \left(\frac{e^{-\mu_B r}}{r} - \frac{e^{-\mu'_B r}}{r} \right), \quad (6)$$

for the Born term $B_{VN,\gamma N}(W)$ (Fig. 1) and

$$v_{cN}^{\text{FSI}}(r) = \alpha_{\text{FSI}} \left(\frac{e^{-\mu_{\text{FSI}} r}}{r} - \frac{e^{-\mu'_{\text{FSI}} r}}{r} \right), \quad (7)$$

for the $J/\psi N$ potential $v_{VN,VN}$ (Fig. 2). In Eqs. (6)–(7), we have defined $\mu'_B = N_B \times \mu_B$ and $\mu'_{\text{FSI}} = N_{\text{FSI}} \times \mu_{\text{FSI}}$. The Pom-CQM model was explained in more detail in Refs. [1, 11] and in Appendix.

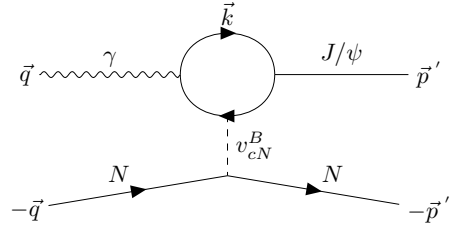


FIG. 1. Born term of the J/ψ photo-production on the nucleon target.

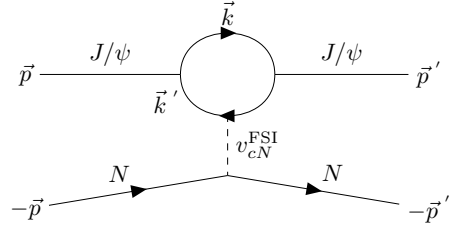


FIG. 2. $J/\psi N$ potential defined by the quark-nucleon potential v_{cN} .

The best fits [11] to the JLab data of the J/ψ photo-production on the proton target are obtained from the so-called fit1 model with the parameters

$$\begin{aligned} \alpha_B &= -0.145; \alpha_{\text{FSI}} = -0.1, \\ \mu_B &= 0.3 \text{ GeV}; \mu_{\text{FSI}} = 0.3 \text{ GeV}, \\ N_B &= 5; N_{\text{FSI}} = 2, \\ F_V(t) &= 1, \end{aligned} \quad (8)$$

where $F_V(t)$ is the form factor of J/ψ defined in Eq. (69) in Appendix.

Figure 3 presents the resulting total cross section of $\gamma p \rightarrow J/\psi p$ as a function of W (a) from threshold up to $W = 300$ GeV and (b) at low energies ($4.0 \leq W \leq 5.9$ GeV). The Pomeron exchange is in excellent agreement with the high energy data ($10 \leq W \leq 300$ GeV) [35–39]

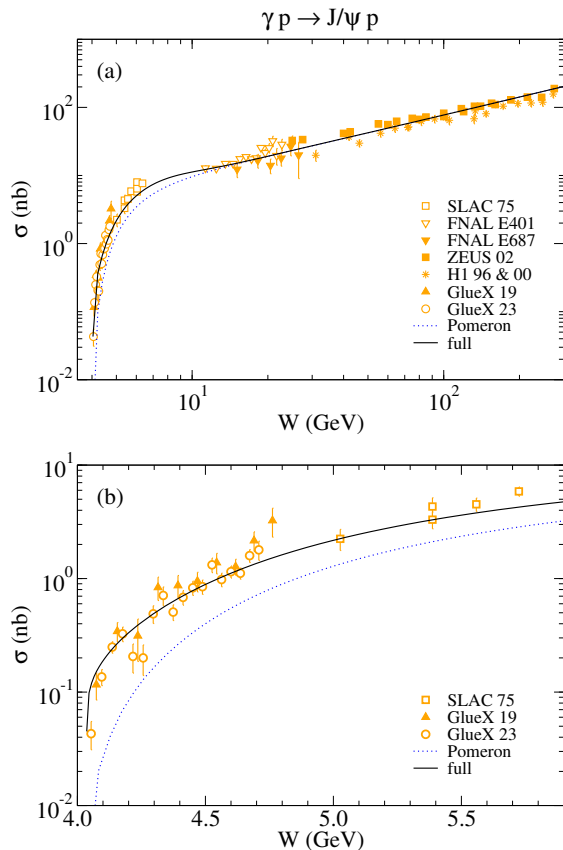


FIG. 3. (a) Total cross section of $\gamma p \rightarrow J/\psi p$ is plotted as a function of the photon c.m. energy from threshold up to $W = 300$ GeV. (b) Total cross section at low energies ($4.0 \leq W \leq 5.9$ GeV). The SLAC [40], FermiLab [35, 36], ZEUS [37], H1 [38, 39], and GlueX [2, 3] data are compared with the Pomeron-exchange (dotted curves) and full (solid curves) contributions [11].

but is not sufficient for describing the low energy region [2, 3, 40]. The full result includes the contribution from the dynamical scattering amplitude $T_{VN,\gamma N}^D(W)$ in Eq. (2) such that the low energy data can be well described.

In Fig. 4, the differential cross sections of $\gamma p \rightarrow J/\psi p$ are displayed as functions of $-t$ at different photon energies $8.90 \leq E_\gamma \leq 10.90$ GeV. The shapes of the Pomeron exchange are too steep to reproduce the available data. The full results agree well with the JLab data [2–4]. Thus the fit1 model in Ref. [11] is suitable for developing an approach to investigate J/ψ photo-production on nuclei.

III. FORMULATION OF EXCLUSIVE J/ψ PHOTO-PRODUCTION ON NUCLEI

The differential cross section of the exclusive photo-production of J/ψ (V) on the nuclear target A , $\gamma(\mathbf{q}, \lambda) + A(\mathbf{P}, M_A) \rightarrow V(\mathbf{k}, m_V) + A(\mathbf{P}', M'_A)$, in the Laboratory

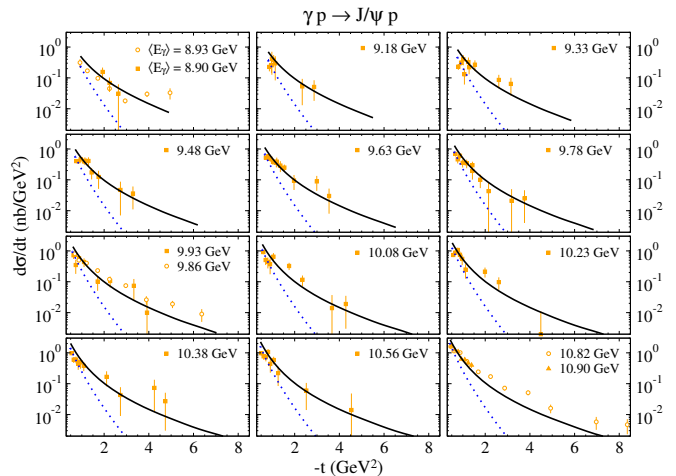


FIG. 4. Differential cross sections of $\gamma p \rightarrow J/\psi p$ are plotted as functions of the momentum transfer $-t$ at different photon energies $8.90 \leq E_\gamma \leq 10.90$ GeV. The GlueX19 [2] (triangle), GlueX23 [3] (circle), and Hall C [4] (quadrangle) data from JLab are compared with the Pomeron-exchange (dotted curves) and full (solid curves) contributions [11].

(Lab) frame ($\mathbf{P} = 0$), can be written as

$$\frac{d\sigma}{d\Omega_{\text{Lab}}} = \rho_A(\mathbf{k}, \mathbf{q}) \frac{1}{2} \frac{1}{2J_A + 1} \sum_{M'_A, M_A} \sum_{m_V, \lambda} |\langle \mathbf{k} m_V, \Phi_{\mathbf{P}', M'_A}^{J_A} | T_{VA, \gamma A}(E) | \mathbf{q} \lambda, \Phi_{\mathbf{P}, M_A}^{J_A} \rangle|^2, \quad (9)$$

where λ is the photon helicity, J_A is the spin of the nucleus A , M_A and m_V are the z -components of the spins of A and V , respectively, and

$$\rho_A(\mathbf{k}, \mathbf{q}) = \frac{(2\pi)^4 |\mathbf{k}|^2 E_V(\mathbf{k}) E_A(\mathbf{q} - \mathbf{k})}{|E_A(\mathbf{q} - \mathbf{k}) |\mathbf{k}| + E_V(\mathbf{k}) (|\mathbf{k}| - |\mathbf{q}| \cos \theta_k)|}. \quad (10)$$

Here \mathbf{q} is in the z -direction and $\cos \theta_k = \hat{\mathbf{q}} \cdot \hat{\mathbf{k}}$.

We will make predictions of the cross sections of the $\gamma A \rightarrow J/\psi A$ reaction using the multiple scattering theory [21–25]. In the distorted-wave impulse approximation [23], the reaction amplitude can be written as

$$T_{VA, \gamma A}(E) = T_{VA, \gamma A}^{\text{IMP}}(E) + T_{VA, \gamma A}^{\text{FSI}}(E). \quad (11)$$

The impulse (IMP) amplitude is given by

$$T_{VA, \gamma A}^{\text{IMP}}(E) = \langle \Phi_A | \sum_{i=1, A} t_{VN, \gamma N}(i) | \Phi_A \rangle, \quad (12)$$

where Φ_A is the wave function of a nucleus with A nucleons and $t_{VN, \gamma N}(i)$ is the amplitude of $\gamma N \rightarrow J/\psi N$ on the i -th nucleon. The FSI amplitude takes the form

$$T_{VA, \gamma A}^{\text{FSI}}(E) = T_{VA, VA}^{(1)}(E) \frac{1}{E - H_0 + i\epsilon} T_{VA, \gamma A}^{\text{IMP}}(E), \quad (13)$$

where H_0 is the free Hamiltonian and $T_{VA,VA}^{(1)}(E)$ is the $J/\psi A \rightarrow J/\psi A$ scattering amplitude calculated from the first-order optical potential $U_{VA,VA}^{(1)}$ using the following Lippmann-Schwinger equation

$$T_{VA,VA}^{(1)}(E) = U_{VA,VA}^{(1)} + U_{VA,VA}^{(1)} \frac{1}{E - H_0 + i\epsilon} T_{VA,VA}^{(1)}(E). \quad (14)$$

Here the first order optical potential is given by [21, 22]

$$U_{VA,VA}^{(1)} = \langle \Phi_A | \sum_{i=1,A} t_{VN,VA}(i) | \Phi_A \rangle, \quad (15)$$

where $t_{VN,VA}(i)$ is the amplitude of $J/\psi N \rightarrow J/\psi N$ on the i -th nucleon.

In Sec. IV, we first consider the simplest nucleus, the deuteron (d), to develop a formulation within which the impulse amplitude of Eq. (12) can be calculated exactly using the deuteron wave function generated from the realistic nucleon-nucleon (NN) potentials [41–43]. We then examine the extent to which the approach based on the fixed scatter approximation (FSA) [21–24] is valid for J/ψ photo-production. In Sec. V, the developed FSA formulation is applied to calculate the first-order optical potential of Eq. (15) and the cross sections of the exclusive J/ψ photo-production on ${}^4\text{He}$, ${}^{16}\text{O}$, and ${}^{40}\text{Ca}$.

IV. PRODUCTION ON THE DEUTERON (d) TARGET

A. Impulse term

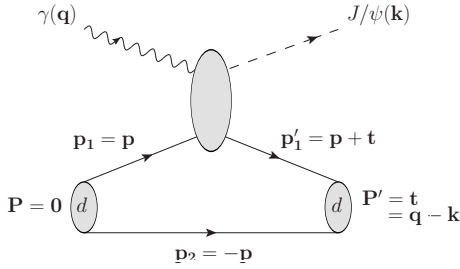


FIG. 5. Diagrammatic representation of $\gamma d \rightarrow J/\psi d$.

We first consider the impulse amplitude in Eq. (11) for $\gamma(\mathbf{q}) + d(\mathbf{P}) \rightarrow J/\psi(\mathbf{k}) + d(\mathbf{P}')$. The momenta of the involved particles are shown in Fig. 5. Including the spin quantum numbers, Eq. (12) can be expressed as

$$\begin{aligned} & \langle \mathbf{k} m_V, \Phi_{\mathbf{P}',M_d'}^{J_d} | T_{Vd,\gamma d}^{\text{IMP}}(E) | \mathbf{q} \lambda, \Phi_{\mathbf{P},M_d}^{J_d} \rangle \\ &= \sum_{i=1}^2 \langle \Phi_{\mathbf{P}',M_d'}^{J_d} | \langle \mathbf{k} m_V | t_{VN,\gamma N}(i) | \mathbf{q} \lambda \rangle | \Phi_{\mathbf{P},M_d}^{J_d} \rangle, \quad (16) \end{aligned}$$

where $\langle \mathbf{k} m_V | t_{VN,\gamma N}(i) | \mathbf{q} \lambda \rangle$ is the J/ψ photo-production amplitude on the i -th nucleon in the deuteron. The deuteron wave function is generated from the available NN potentials [41–43] and is defined by

$$\begin{aligned} & \Phi_{\mathbf{P},M_d}^{J_d}(\mathbf{p}_1 m_{s_1}, \mathbf{p}_2 m_{s_2}) \\ &= \delta(\mathbf{P} - \mathbf{p}_1 - \mathbf{p}_2) \Gamma(\mathbf{P}\mathbf{p}, \mathbf{p}_1\mathbf{p}_2) \phi_{M_d}^{J_d}(\mathbf{p}, m_{s_1} m_{s_2}), \quad (17) \end{aligned}$$

where m_{s_i} is the z -component of the spin of the i -th nucleon, \mathbf{P} is the total momentum of d , \mathbf{p}_i is the momentum of the i -th nucleon, and $\Gamma(\mathbf{P}\mathbf{p}, \mathbf{p}_1\mathbf{p}_2)$ is the transformation coefficient from the momenta $(\mathbf{p}_1, \mathbf{p}_2)$ in the Lab frame to (\mathbf{P}, \mathbf{p}) in the rest frame of the deuteron. The momentum variables in Eq. (17) are explicitly defined by

$$\mathbf{P} = \mathbf{p}_1 + \mathbf{p}_2, \quad (18)$$

$$\mathbf{p} = \frac{1}{2}(\mathbf{p}_1 - \mathbf{p}_2), \quad (19)$$

$$\begin{aligned} \Gamma(\mathbf{P}\mathbf{p}, \mathbf{p}_1\mathbf{p}_2) &= \langle \mathbf{p}_1\mathbf{p}_2 | \mathbf{P}\mathbf{p} \rangle \\ &= \sqrt{\frac{\partial(\mathbf{P}, \mathbf{p})}{\partial(\mathbf{p}_1, \mathbf{p}_2)}}. \quad (20) \end{aligned}$$

With the nonrelativistic kinematics in Eqs. (18)-(19), the transformation coefficient of Eq. (20) obviously becomes

$$\Gamma(\mathbf{P}\mathbf{p}, \mathbf{p}_1\mathbf{p}_2) = 1. \quad (21)$$

In Eq. (17), $\phi_{M_d}^{J_d}(\mathbf{p}, m_{s_1} m_{s_2})$ is the wave function in the rest frame ($\mathbf{P} = 0$) of the deuteron and takes the form

$$\begin{aligned} \phi_{M_d}^{J_d}(\mathbf{p}, m_{s_1} m_{s_2}) &= \sum_{L, M_L, M_S} \langle J_d M_d | L S M_L M_S \rangle \\ &\times \langle S M_S | \frac{1}{2} m_{s_1} m_{s_2} \rangle Y_{L M_L}(\hat{p}) R_L(|\mathbf{p}|), \quad (22) \end{aligned}$$

where $J_d = 1$, $S = 1$, L is the relative orbital angular momentum of the two nucleons in d , and $R_L(|\mathbf{p}|)$ is the radial part of the deuteron wave function.

Using the deuteron wave function given in Eq. (17) and noting that

$$\Gamma(\mathbf{0}\mathbf{p}, \mathbf{p}_1\mathbf{p}_2) = 1, \quad (23)$$

Eq. (16) can be written as

$$\begin{aligned} & \langle \mathbf{k} m_V, \Phi_{\mathbf{P}',M_d'}^{J_d} | T_{Vd,\gamma d}^{\text{IMP}}(E) | \mathbf{q} \lambda, \Phi_{\mathbf{P},M_d}^{J_d} \rangle = \\ & \sum_{m_{s_1}, m_{s_2}, m_{s_1'}, m_{s_2}'} A_d \int d\mathbf{p} \phi_{M_d'}^{J_d*}(\mathbf{p}', m_{s_1'} m_{s_2}') \\ & \times \Gamma(\mathbf{P}'\mathbf{p}', \mathbf{p}_1'\mathbf{p}_2') \phi_{M_d}^{J_d}(\mathbf{p}, m_{s_1} m_{s_2}) \\ & \times \langle \mathbf{k} m_V, \mathbf{p}_1' m_{s_1}' | t_{VN,\gamma N}(\omega) | \mathbf{q} \lambda, \mathbf{p} m_{s_1} \rangle, \quad (24) \end{aligned}$$

where $A_d = 2$ is the number of the nucleons in the deuteron. As illustrated in Fig. 5, the momentum variables in Eq. (24) are defined in the Lab frame by

$$\mathbf{p}_1 = \mathbf{p}; \mathbf{p}_2 = -\mathbf{p}, \quad (25)$$

$$\mathbf{p}_1' = \mathbf{p} + \mathbf{t}; \mathbf{p}_2' = -\mathbf{p}, \quad (26)$$

where $\mathbf{t} = \mathbf{q} - \mathbf{k}$ and

$$\mathbf{p}' = \frac{1}{2}(\mathbf{p}'_1 - \mathbf{p}'_2) = \mathbf{p} + \frac{1}{2}\mathbf{t}. \quad (27)$$

By setting $\Gamma(\mathbf{P}'\mathbf{p}', \mathbf{p}'_1\mathbf{p}'_2) = 1$, as given in Eq. (21), Eqs. (24)-(27) are for the nonrelativistic calculations of the impulse amplitude.

The main feature of the J/ψ photo-production at energies near the threshold is that the momentum transfer $-t$ is very large. For example, the contributions to the cross sections at photon energy $E_\gamma = 6$ GeV are from the $-t \geq 2$ GeV² region where the relativistic effects are expected to be important. We therefore follow Refs. [44–48] to modify the above nonrelativistic formula to account for relativistic effects using the instant form of Relativistic Quantum Mechanics [49, 50].

The main step is to replace the relative momentum \mathbf{p} of Eq. (19) by the following expression

$$\mathbf{p} = L(\vec{\beta})\mathbf{p}_1 = -L(\vec{\beta})\mathbf{p}_2, \quad (28)$$

where $L(\vec{\beta})$ is the Lorentz Boost transformation with the velocity defined by

$$\vec{\beta} = \frac{\mathbf{P}}{E_N(\mathbf{p}_1) + E_N(\mathbf{p}_2)}. \quad (29)$$

It can be shown [48, 50] that for a particle with momentum \mathbf{p}_i and mass m

$$L(\vec{\beta})\mathbf{p}_i = \mathbf{p}_i + \gamma \left[\frac{\gamma}{1+\gamma} (\vec{\beta} \cdot \mathbf{p}_i) - E_m(\mathbf{p}_i) \right], \quad (30)$$

where $\gamma = 1/\sqrt{1-\vec{\beta}^2}$ and $E_m(\mathbf{p}_i) = \sqrt{\mathbf{p}_i^2 + m^2}$. Using \mathbf{P} of Eq. (18) and \mathbf{p} of Eqs. (28)-(30), one can show that [50] the transformation coefficient of Eq. (20) becomes

$$\Gamma(\mathbf{P}\mathbf{p}, \mathbf{p}_1\mathbf{p}_2) = \left[\frac{E_1(\mathbf{p}_1) + E_2(\mathbf{p}_2)}{E_1(\mathbf{p}) + E_2(\mathbf{p})} \frac{E_1(\mathbf{p})E_2(\mathbf{p})}{E_1(\mathbf{p}_1)E_2(\mathbf{p}_2)} \right]^{\frac{1}{2}}. \quad (31)$$

Relativistic effects can be included using the same equations of Eqs. (24)-(27) but using Eq. (31) to evaluate $\Gamma(\mathbf{P}'\mathbf{p}', \mathbf{p}'_1\mathbf{p}'_2)$ and replacing \mathbf{p}' of Eq. (27) by

$$\mathbf{p}' = L(\vec{\beta}')\mathbf{p}'_1 = -L(\vec{\beta}')\mathbf{p}'_2, \quad (32)$$

where

$$\vec{\beta}' = \frac{\mathbf{t}}{E_N(\mathbf{p}'_1) + E_N(\mathbf{p}'_2)}. \quad (33)$$

In addition to the above relativistic extension, the spin rotations under Lorentz Boost transformation are also needed to have a complete relativistic approach. However, it was found in Refs. [44, 45, 48] that the spin rotations have negligible effects on the spin-averaged observables which are only considered in this work. Thus we will not account for this complication for simplicity.

The resulting total cross section of $\gamma d \rightarrow J/\psi d$ is depicted in Fig. 6 as a function of E_γ (a) from threshold up to $E_\gamma = 25$ GeV and (b) at low energies ($6 \leq E_\gamma \leq 7$ GeV). The results using the nonrelativistic and relativistic formulation of the deuteron wave function are compared to each other. We see that their differences are very large near the threshold region and are much less at higher energies.

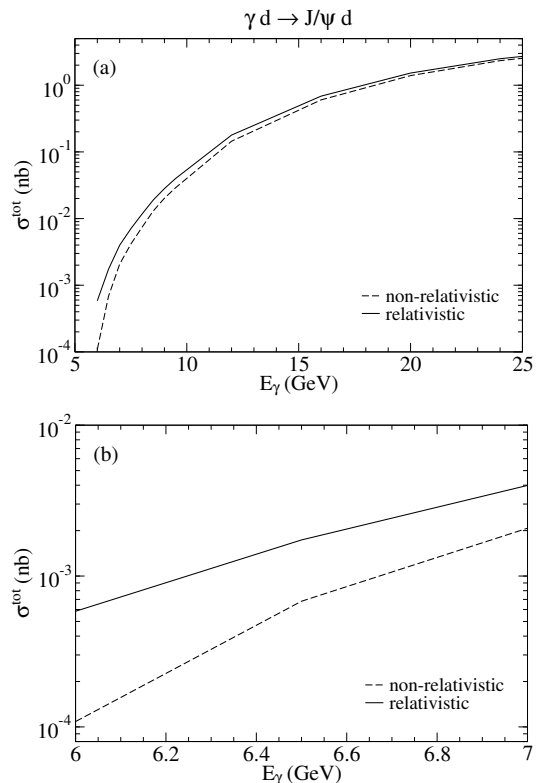


FIG. 6. (a) Total cross section of $\gamma d \rightarrow J/\psi d$ is plotted as a function of the photon Lab energy from threshold up to $E_\gamma = 25$ GeV. (b) Total cross section at low energies ($6 \leq E_\gamma \leq 7$ GeV). The results using the nonrelativistic (dashed curves) and relativistic (solid curves) formulation of the deuteron wave function are compared.

This can be understood from Fig. 7 where the differential cross sections are presented as functions of $-t$. At $E_\gamma = 6$ GeV (a), which is about 0.4 GeV above the threshold, the results using the relativistic deuteron wavefunction are about an order of magnitude larger than those using the nonrelativistic one in the large momentum-transfer region of $-t \geq 1.8$ GeV². As the photon energy increases, the total cross sections are mainly from the low momentum-transfer region where the relativistic effects are not large as seen in Fig. 7(b)-(c).

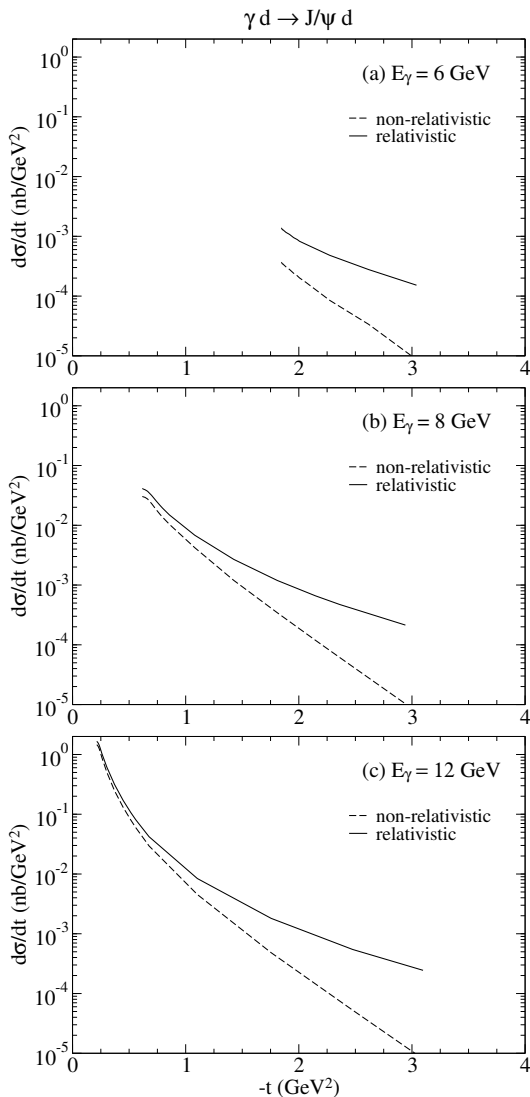


FIG. 7. Differential cross sections of $\gamma d \rightarrow J/\psi d$ at $E_\gamma = (6, 8, 10)$ GeV. The results using the nonrelativistic (dashed curves) and relativistic (solid curves) formulation of the deuteron wave function are compared.

B. Fixed scatter approximation (FSA)

For understanding the results of differential cross sections shown in Fig. 7, it is useful to use an approximation to relate Eq. (24) to the nuclear form factors which characterize the structure of the deuteron. This can be done using the FSA [21–24] to set the initial nucleon momentum to be $\mathbf{p} = 0$ in the amplitude $\langle \mathbf{k} m_V, \mathbf{p}'_1 m_{s'_1} | t_{VN, \gamma N}(\omega) | \mathbf{q} \lambda, \mathbf{p} m_{s_1} \rangle$ and also to set the transformation coefficient $\Gamma(\mathbf{P}' \mathbf{p}', \mathbf{p}'_1 \mathbf{p}'_2) = 1$. Eq. (24) can then be approximately written as the following factorized form

$$\langle \mathbf{k} m_V, \Phi_{\mathbf{P}'_1, M'_d}^{J_d} | T_{VN, \gamma d}^{\text{IMP}}(E) | \mathbf{q} \lambda, \Phi_{\mathbf{P}, M_d}^{J_d} \rangle \sim A_d(\mathbf{k} m_V, \mathbf{t} \bar{m}_{s'_1} | \bar{t}_{VN, \gamma N}(\omega_0) | \mathbf{q} \lambda, \mathbf{0} \bar{m}_{s_1}) F_{M'_d, M_d}(t), \quad (34)$$

where \bar{m}_{s_1} and $\bar{m}_{s'_1}$ are arbitrarily chosen spin components, $t = (|\mathbf{q}| - E_V(\mathbf{k}))^2 - \mathbf{t}^2$, and

$$F_{M'_d, M_d}(t) = \sum_{m_{s_1}, m_{s_2}, m_{s'_1}, m_{s'_2}} \int d\mathbf{p} \phi_{M'_d}^{J_d*}(\mathbf{p} + \frac{\mathbf{t}}{2}, m_{s'_1} m_{s'_2}) \phi_{M_d}^{J_d}(\mathbf{p}, m_{s_1} m_{s_2}). \quad (35)$$

By choosing \mathbf{t} in the z -direction, one can show that

$$\begin{aligned} F_{0,0}(t) &= \sqrt{4\pi}[F_0(t) - \sqrt{2}F_2(t)], \\ F_{1,1}(t) &= F_{-1,-1}(t) = \sqrt{4\pi}[F_0(t) + \frac{1}{\sqrt{2}}F_2(t)], \\ F_{M'_d, M_d}(t) &= 0 \text{ if } M'_d \neq M_d, \end{aligned} \quad (36)$$

where $F_L(t)$ with $L = (0, 2)$ are the deuteron form factors. Eqs. (34)–(36) imply that the reaction cross sections are closely related to the deuteron form factors. In Fig. 8, we show the deuteron form factors generated from the Argonne-V18 potential [41]. We see that the quadrupole form factor $F_2(t)$ peaks in the region where $F_0(t)$ has a minimum. It is clear that the reaction cross sections at large $-t$ depend strongly on $F_2(t)$ which is due to the d -state of the wave function.

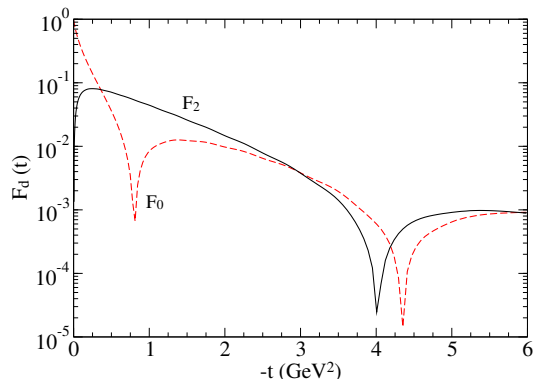


FIG. 8. Deuteron form factors calculated using the deuteron wave function from the Argonne-V18 NN potential [41].

The dependence of the cross sections calculated using the relativistic form of Eq. (24) is expected to be similar to that discussed above using the FSA of Eqs. (34)–(36). To see how the d -state can be probed by the J/ψ exclusive production process, we compare in Fig. 9 the full results, which correspond to the solid curves in Fig. 7, with results obtained by keeping only the s -wave part of the deuteron wave function in the calculations using the relativistic form of Eq. (24). At $E_\gamma = 6$ GeV (a) which is close to the threshold, both results of $d\sigma/dt$ have no minimum because they only cover the region of large $-t$ where both $F_0(t)$ and $F_2(t)$ have no minimum. In the same $-t$ region, $F_2(t)$ is larger than $F_0(t)$ and hence the results from keeping only the s -wave part of the deuteron wave function are much smaller. At higher energies, the small $-t$ region is covered and the cross sections from only the

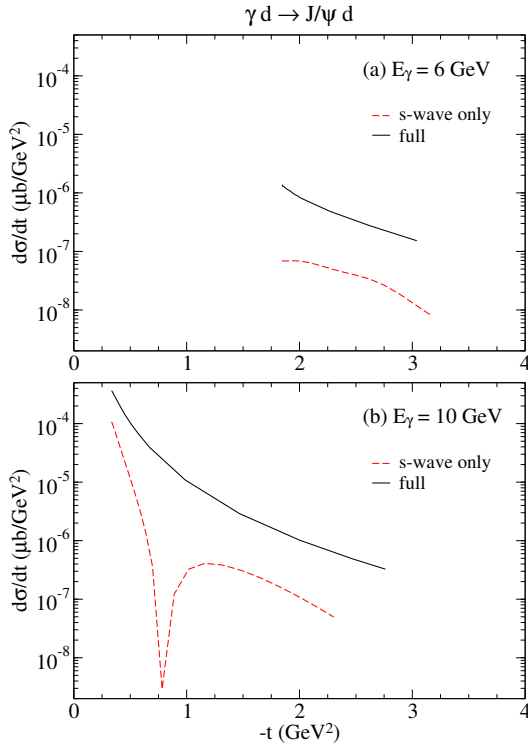


FIG. 9. Differential cross sections of $\gamma d \rightarrow J/\psi d$ at $E_\gamma = (6, 10)$ GeV. The results using only the s -wave part (dashed curves) and using all parts (solid curves) of the deuteron wave function are compared. (Note that the unit for $d\sigma/dt$ in this figure is in $\mu\text{b}/\text{GeV}^2$.)

s -wave part of the deuteron wavefunction have a minimum similar to that of $F_0(t)$ as displayed in Fig. 9(b). Thus the production near the threshold is very effective in testing the d -state of the deuteron wave function.

The FSA is useful in practice and will be used later in calculating the FSI term and the cross sections for the production on heavier nuclei. Therefore we need to examine the extent to which it is valid. The results can be understood clearly in calculations keeping only the s -wave part of the deuteron wavefunction, such that the cross sections only depend on one form factor $F_0(t)$. Using the relativistic form, the FSA results can be obtained by simply setting the initial nucleon momentum $\mathbf{p} = 0$ in Eq. (24). The resulting differential cross sections (solid curves) are depicted in Fig. 10 where the dashed curves correspond to the dashed curves in Fig. 9. The FSA is found to be a good approximation only in the small $-t$ region. Thus the FSA is not valid at energies near the threshold where the cross sections are only from the large $-t$ region, as shown in Fig. 10(a). On the other hand, the FSA is reasonable at higher energies $E_\gamma = 8$ (b) and 10 (c) GeV.

The FSA is employed in Ref. [26] for ϕ photo-production on the spin $J = 0$ nucleus ${}^4\text{He}$ and will be used in our later calculations for heavier nuclei. It

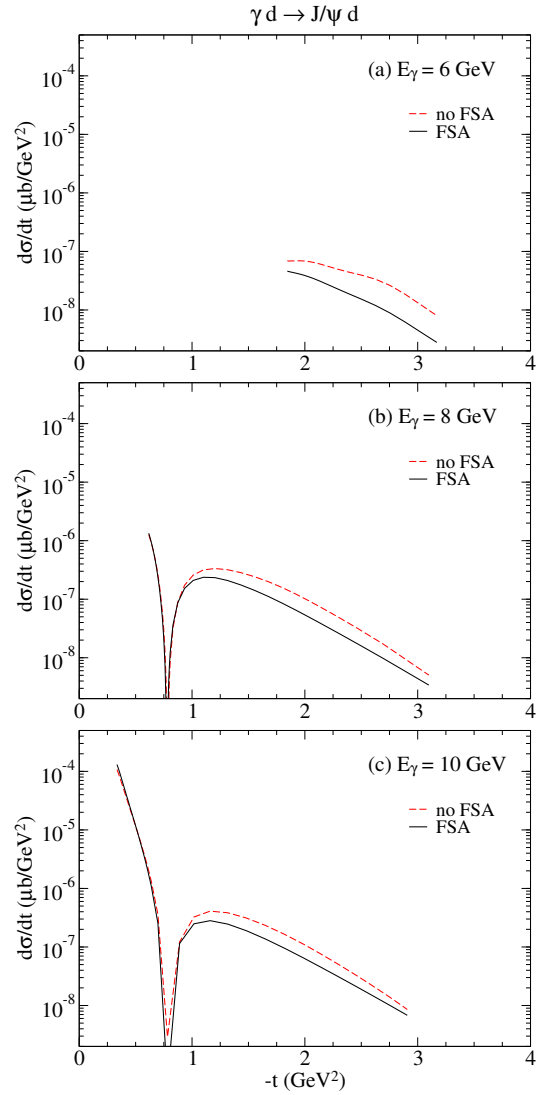


FIG. 10. Differential cross sections of $\gamma d \rightarrow J/\psi d$ at $E_\gamma = (6, 8, 10)$ GeV. The results using the FSA (solid curves) are compared with the exact results (dashed curves). (Note that the unit for $d\sigma/dt$ in this figure is in $\mu\text{b}/\text{GeV}^2$.)

is therefore useful to see how it can be derived from Eq. (34). To proceed, we need to first specify the undefined spin components \bar{m}_s and \bar{m}'_s in Eq. (34). It is reasonable to follow the expression for the production cross sections on the nucleon to define the averaged amplitude in Eq. (34) as

$$\begin{aligned} & |\langle \mathbf{k}m_V, \mathbf{t}\bar{m}'_{s'_1} | \bar{t}_{Vd,\gamma d}(\omega_0) | \mathbf{q}\lambda, \mathbf{0}\bar{m}_{s_1} \rangle|^2 \\ &= \frac{1}{2} \sum_{m_{s'_1}, m_{s_1}} |\langle \mathbf{k}m_V, \mathbf{t}m_{s'_1} | t_{VN,\gamma N}(\omega) | \mathbf{q}\lambda, \mathbf{0}m_{s_1} \rangle|^2. \end{aligned} \quad (37)$$

This allows us to cast Eq. (9) into the following FSA form

$$\left(\frac{d\sigma}{d\Omega_{\text{Lab}}}\right)_{\text{FSA}} = \rho_d(\mathbf{k}, \mathbf{q}) \frac{1}{4} \sum_{m_{s'_1}, m_{s_1}, m_V, \lambda} \times |\langle \mathbf{k}m_V, \mathbf{t}m_{s'_1} | T_{Vd, \gamma d}^{\text{FSA}}(\omega) | \mathbf{q}\lambda, \mathbf{0}m_{s_1} \rangle|^2, \quad (38)$$

where

$$\langle \mathbf{k}m_V, \mathbf{t}m_{s'_1} | T_{Vd, \gamma d}^{\text{FSA}}(\omega) | \mathbf{q}\lambda, \mathbf{0}m_{s_1} \rangle = A_d \langle \mathbf{k}m_V, \mathbf{t}m_{s'_1} | t_{VN, \gamma N}(\omega) | \mathbf{q}\lambda, \mathbf{0}m_{s_1} \rangle F_{ave}(t) \quad (39)$$

Here we used the properties of Eq. (36) to define

$$F_{ave}(t) = \frac{1}{\sqrt{4\pi}} \left[\frac{1}{2J_d + 1} \sum_{M_d, M_d'} |F_{M_d', M_d}|^2 \right]^{\frac{1}{2}} = [F_0(t)^2 + F_2(t)^2]^{\frac{1}{2}}. \quad (40)$$

The FSA defined by Eqs. (38)-(39) is the same as the formulation employed in Ref. [26] for ϕ photo-production on the spin $J = 0$ nucleus ${}^4\text{He}$.

C. Final state interactions

We now turn to investigating the effects of the FSI term $T_{Vd, \gamma d}^{\text{FSI}}(E)$ in Eq. (11). As defined in Eq. (13), we need to evaluate the following matrix element

$$\langle \mathbf{k}m_V, \Phi_{\mathbf{P}', M_d'}^{J_d} | T_{Vd, \gamma d}^{\text{FSI}}(E) | \mathbf{q}\lambda, \Phi_{\mathbf{P}, M_d}^{J_d} \rangle = \sum_{\bar{m}_V, \bar{M}_d} \int d\mathbf{k}' \langle \mathbf{k}m_V, \Phi_{\mathbf{P}', M_d'}^{J_d} | T_{Vd, Vd}^{(1)}(E) | \mathbf{k}'\bar{m}_V, \Phi_{\bar{\mathbf{P}}, \bar{M}_d}^{J_d} \rangle \times \frac{1}{E - E_V(k') - E_d(\bar{\mathbf{P}}) + i\epsilon} \times \langle \mathbf{k}'\bar{m}_V, \Phi_{\bar{\mathbf{P}}, \bar{M}_d}^{J_d} | T_{Vd, \gamma d}^{\text{IMP}}(E) | \mathbf{q}\lambda, \Phi_{\mathbf{P}, M_d}^{J_d} \rangle, \quad (41)$$

where $\bar{\mathbf{P}} = \mathbf{P} + \mathbf{q} - \mathbf{k}'$.

The matrix element of $T_{Vd, Vd}^{(1)}(E)$ in the above equation is defined by Eqs. (14)-(15). We follow the previous works [21-24] to use the FSA to calculate the first-order optical potential $U_{Vd, Vd}^{(1)}$ and solve the scattering equation of Eq. (14) in the V - d c.m. frame. Eq. (15) then leads to the following matrix element (omitting the spin indices)

$$\langle \mathbf{p} | U_{Vd, Vd}^{(1)} | \mathbf{p}' \rangle = \langle \kappa | t_{VN, VN} | \kappa' \rangle F_T(t'), \quad (42)$$

where $t' = (p' - p)^2$ and \mathbf{p}' (\mathbf{p}) is the initial (final) momentum of J/ψ in the V - d c.m. system in which a frozen nucleon in the deuteron is in the opposite direction with the momentum $-\mathbf{p}'/A_d$ ($-\mathbf{p}/A_d$). We need to use the Lorentz Boost transformation (see Eq. (30)) to evaluate κ' (κ), which is the momentum of J/ψ in the initial (final) V - N c.m. system, from the ($J/\psi, N$) momenta ($\mathbf{p}', -\mathbf{p}'/A_d$) ($\mathbf{p}, -\mathbf{p}/A_d$). The $J/\psi N \rightarrow J/\psi N$

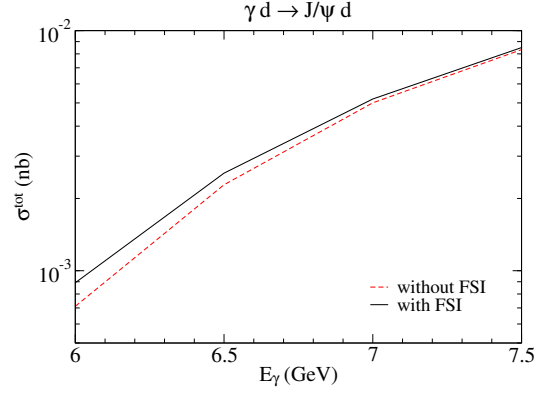


FIG. 11. FSI effects on the total cross section of $\gamma d \rightarrow J/\psi d$. The results without (dashed curve) and with (solid curve) the FSI effects are compared.

scattering amplitude $\langle \kappa | t_{VN, VN} | \kappa' \rangle$ is obtained by solving Eq. (5) using the $J/\psi N$ potential generated from the quark- N potential of Eq. (7). $F_T(t')$ is the nuclear form factor. For the deuteron, we use $F_T(t') = F_{ave}(t')$ of Eq. (40).

As given in Appendix, $\langle \kappa | t_{VN, VN} | \kappa' \rangle$ is calculated from the spin independent quark- N potential of Eq. (7). The spin averaged nuclear form factor $F_T(t') = F_{ave}(t')$ is also independent of spin. Thus the matrix element with spin indices of $U_{Vd, Vd}^{(1)}$ is of the form

$$\langle \mathbf{p}, m_V M_d | U_{Vd, Vd}^{(1)} | \mathbf{p}', m_V' M_d' \rangle = \delta_{m_V, m_V'} \delta_{M_d, M_d'} \langle \mathbf{p} | U_{Vd} | \mathbf{p}' \rangle. \quad (43)$$

Accordingly, the $J/\psi d \rightarrow J/\psi d$ scattering amplitude, defined in Eq. (14), can also be written as

$$\langle \mathbf{p}, m_V M_d | T_{Vd, Vd}^{(1)}(E) | \mathbf{p}', m_V' M_d' \rangle = \delta_{m_V, m_V'} \delta_{M_d, M_d'} \langle \mathbf{p} | T_{Vd}(E) | \mathbf{p}' \rangle, \quad (44)$$

where $\langle \mathbf{p} | T_{Vd}(E) | \mathbf{p}' \rangle$ is defined by the following Lippmann-Schwinger equation

$$\langle \mathbf{p} | T_{Vd}(E) | \mathbf{p}' \rangle = \langle \mathbf{p} | U_{Vd} | \mathbf{p}' \rangle + \int d\mathbf{p}'' \frac{\langle \mathbf{p} | U_{Vd} | \mathbf{p}'' \rangle \langle \mathbf{p}'' | T_{Vd}(E) | \mathbf{p}' \rangle}{E - E_V(p'') - E_d(p'') + i\epsilon}. \quad (45)$$

We solve Eq. (45) by using the standard numerical method described in Ref. [51].

Note that Eq. (41) is given in the Lab frame. Following Ref. [50], the J/ψ - d scattering amplitude in Eq. (41) is then calculated from Eq. (44) by

$$\langle \mathbf{k}m_V, \Phi_{\mathbf{P}', M_d'}^{J_d} | T_{Vd, Vd}^{(1)}(E) | \mathbf{k}'\bar{m}_V, \Phi_{\bar{\mathbf{P}}, \bar{M}_d}^{J_d} \rangle = \delta_{m_V, \bar{m}_V} \delta_{M_d', \bar{M}_d} \langle \mathbf{k}\mathbf{P}' | T_{Vd}(E) | \mathbf{k}'\bar{\mathbf{P}} \rangle, \quad (46)$$

where

$$\langle \mathbf{k}\mathbf{P}' | T_{Vd}(E) | \mathbf{k}'\bar{\mathbf{P}} \rangle = N(\mathbf{p}', \mathbf{k}\mathbf{P}') \langle \mathbf{p}' | T_{Vd}(E) | \bar{\mathbf{p}} \rangle N(\bar{\mathbf{p}}, \mathbf{k}'\bar{\mathbf{P}}), \quad (47)$$

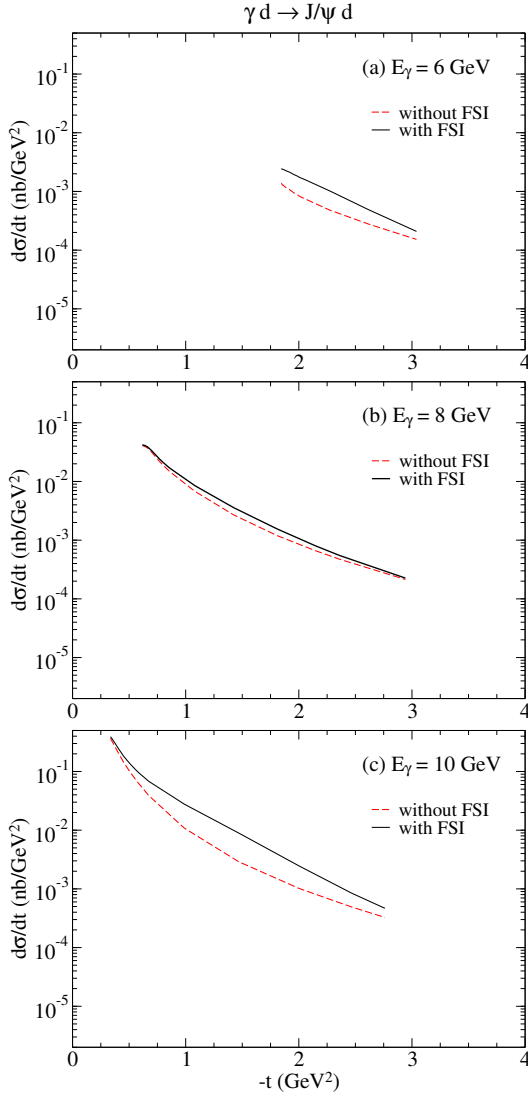


FIG. 12. FSI effects on the differential cross sections of $\gamma d \rightarrow J/\psi d$ at $E_\gamma = (6, 8, 10)$ GeV. The results without (dashed curves) and with (solid curves) the FSI effects are compared at three different photon energies.

with

$$N(\mathbf{p}, \mathbf{p}_1 \mathbf{p}_2) = \left[\frac{E_1(\mathbf{p}_1) + E_2(\mathbf{p}_2)}{E_1(\mathbf{p}) + E_2(\mathbf{p})} \frac{E_1(\mathbf{p}) E_2(\mathbf{p})}{E_1(\mathbf{p}_1) E_2(\mathbf{p}_2)} \right]^{\frac{1}{2}}, \quad (48)$$

where \mathbf{p} is the momentum in the V - d c.m. frame calculated from the momenta \mathbf{p}_1 and \mathbf{p}_2 in the Lab frame. To be consistent with the procedures for calculating $T_{Vd,Vd}^{(1)}(E)$, we use the FSA to evaluate the matrix element of $T_{Vd,\gamma d}^{\text{IMP}}(E)$ in the FSI amplitude of Eq. (41). Namely, $T_{Vd,\gamma d}^{\text{IMP}}(E)$ in Eq. (41) is calculated from Eq. (24) by setting the initial nucleon momentum to be $\mathbf{p} = 0$.

The FSI effects are presented in Fig. 11 where we compare the total cross section of $T_{Vd,\gamma d}^{\text{IMP}}$ (dashed curve) and $T_{Vd,\gamma d}^{\text{IMP}} + T_{Vd,\gamma d}^{\text{FSI}}$ (solid curve). Here $T_{Vd,\gamma d}^{\text{IMP}}$ indicates

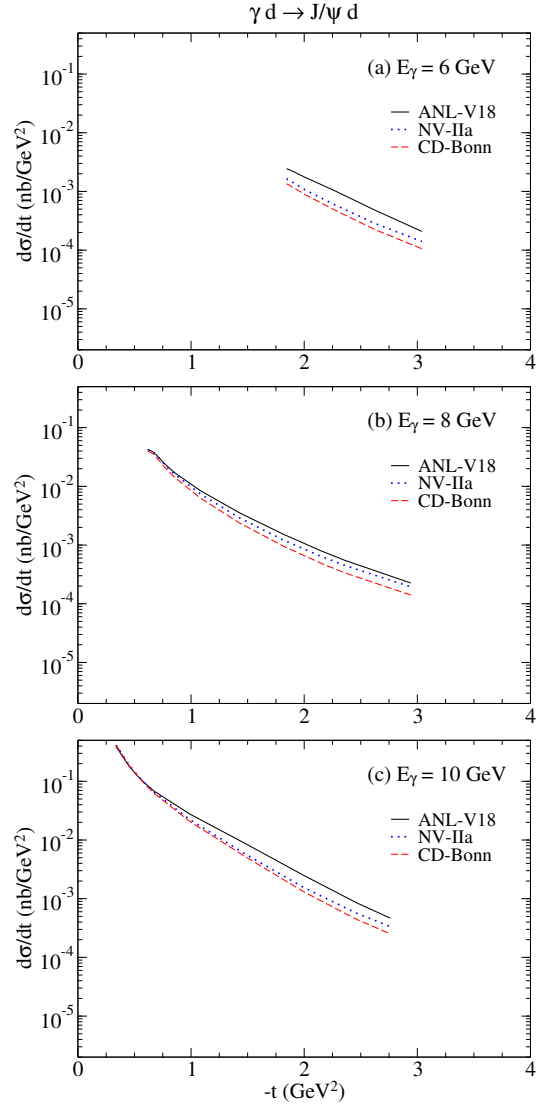


FIG. 13. Differential cross sections of $\gamma d \rightarrow J/\psi d$ at $E_\gamma = (6, 8, 10)$ GeV. The results using the deuteron wave function generated from three different NN potentials [41–43] are compared.

the result obtained from the relativistic formulation of Eq. (24) explained in Sec. IV(A). We see that the FSI effects significantly increase the cross sections at energies near the threshold. This can be understood from the results of the differential cross sections shown in Fig. 12. We find that the FSI amplitude mainly contributes to the large $-t$ region.

For later calculations of the J/ψ photo-production on heavier nuclei in Sec. V, we note here that, if we use Eq. (39) of the FSA to evaluate T^{IMP} of Eq. (41), Eq. (41)

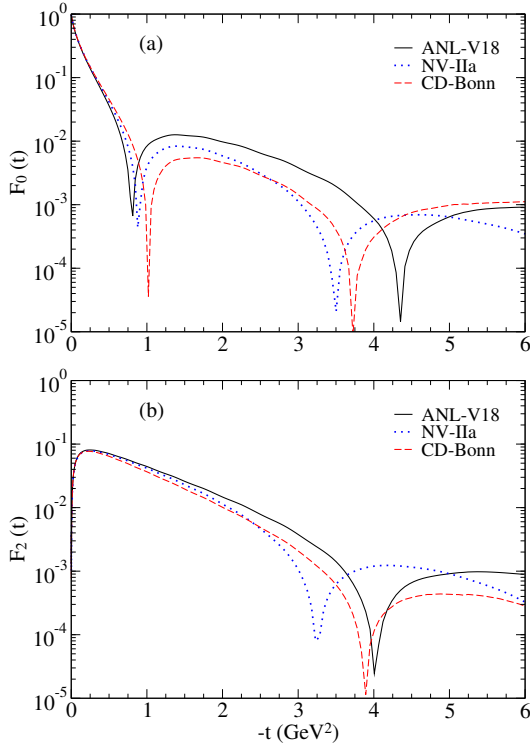


FIG. 14. Deuteron form factors (a) $F_0(t)$ and (b) $F_2(t)$ calculated from the deuteron wave function generated from three different NN potentials [41–43] are compared.

can then be simplified as

$$\begin{aligned} & \langle \mathbf{k}m_V, \Phi_{\mathbf{P}', M_d}^{J_d} | T_{Vd, \gamma d}^{\text{FSI}}(E) | \mathbf{q}\lambda, \Phi_{\mathbf{P}, M_d}^{J_d} \rangle \\ & \sim A_d \langle \mathbf{k}m_V, \mathbf{t}\bar{m}_{s_1'} | t_{VN, \gamma N}(\omega_0) | \mathbf{q}\lambda, \mathbf{0}\bar{m}_{s_1} \rangle \\ & \times F_T^{\text{FSI}}(t) \delta_{M_d', M_d}, \end{aligned} \quad (49)$$

where

$$\begin{aligned} F_T^{\text{FSI}}(t) &= \int d\mathbf{k}' \langle \mathbf{k}\mathbf{P}' | T_{Vd}(E) | \mathbf{k}'\bar{\mathbf{P}} \rangle \\ & \times \frac{1}{E - E_V(k') - E_d(\bar{P}) + i\epsilon} F_{ave}(t). \end{aligned} \quad (50)$$

By using Eqs. (49)-(50), the FSA cross section of Eq. (38) can then be extended to include the FSI term and becomes

$$\begin{aligned} \left(\frac{d\sigma}{d\Omega_{\text{Lab}}} \right)_{\text{FSA}} &= \rho_d(\mathbf{k}, \mathbf{q}) \frac{1}{4} \sum_{m_{s_1'}, m_{s_1}, m_V, \lambda} \\ & \times | \langle \mathbf{k}m_V, \mathbf{t}m_{s_1'} | t_{VN, \gamma N}(\omega) | \mathbf{q}\lambda, \mathbf{0}m_{s_1} \rangle |^2 \\ & \times | A_d [F_{ave}(t) + F_T^{\text{FSI}}(t)] |^2. \end{aligned} \quad (51)$$

D. Model dependence

By using the calculation procedures described in Sec. IV(C), we next investigate how the predicted cross

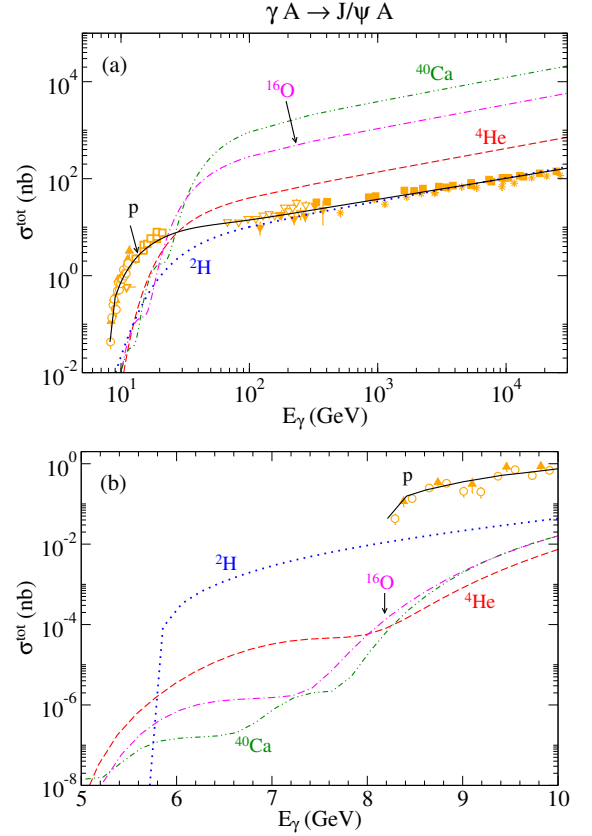


FIG. 15. (a) Total cross sections of $\gamma A \rightarrow J/\psi A$ ($A = p, {}^2\text{H}, {}^4\text{He}, {}^{16}\text{O},$ and ${}^{40}\text{Ca}$) are plotted as a function of E_γ from threshold up to $E_\gamma \sim 10^4$ GeV. (b) Total cross section at low energies ($5 \leq E_\gamma \leq 10$ GeV). The SLAC [40], FermiLab [35, 36], ZEUS [37], H1 [38, 39], and GlueX [2, 3] data are used for $\gamma p \rightarrow J/\psi p$.

sections depend on the NN model used in generating the deuteron wave function. We consider the Argonne-V18 [41], Norfolk NV-IIa [42], and CD-Bonn [43] models. The predicted differential cross sections are compared in Fig. 13. Here the solid curves correspond to the solid curves in Fig. 12. Clearly, their differences are mainly in the large $-t$ region. This can be understood from comparing their form factors, shown in Fig. 14, which are related to their wave function. We see that their differences are also in the large $-t$ region. Obviously, their differences can be clearly distinguished at very near threshold $E_\gamma = 6$ GeV, while it will be very challenging to measure such small cross sections.

V. PRODUCTION ON $J = 0$ NUCLEI

For heavier nuclei, we will use the FSA as developed in the previous section. We only consider the exclusive J/ψ photo-production on the spin $J = 0$ nuclei which have only one nuclear form factor $F_T(t)$. Following Eq. (51),

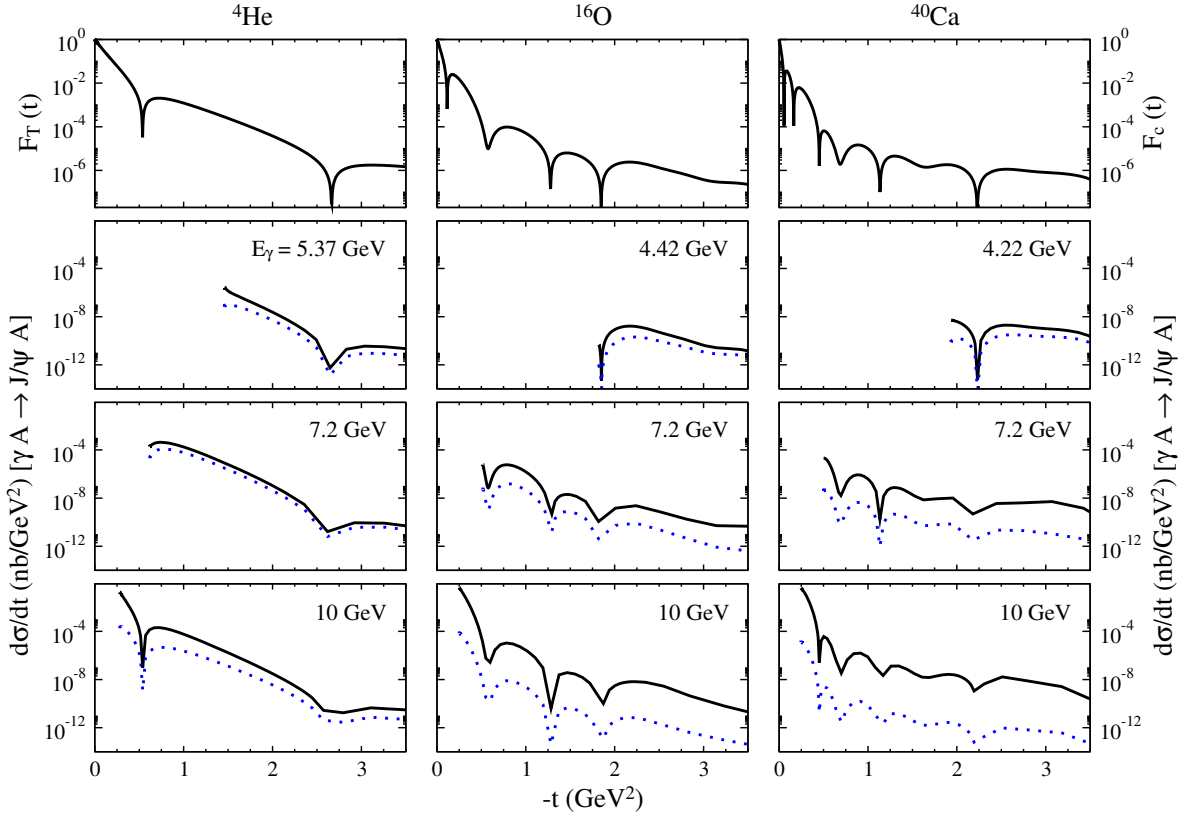


FIG. 16. The top panels show the nuclear form factors of nuclei A ($A = {}^4\text{He}$, ${}^{16}\text{O}$, ${}^{40}\text{Ca}$). Below the top panels, Differential cross sections of $\gamma A \rightarrow J/\psi A$ are presented at $E_\gamma = (E_\gamma^{\text{th}} + 1.0, 7.2, 10)$ GeV. The results of the FSI effects (dotted curves) and the full results (solid curves) are compared.

the differential cross sections for $\gamma(\mathbf{q}) + A \rightarrow J/\psi(\mathbf{k}) + A$ in the Lab frame can be written as

$$\begin{aligned} \frac{d\sigma}{d\Omega_{\text{Lab}}} &= \frac{(2\pi)^4 |\mathbf{k}|^2 E_V(\mathbf{k}) E_A(\mathbf{q} - \mathbf{k})}{|E_A(\mathbf{q} - \mathbf{k})|\mathbf{k}| + E_V(\mathbf{k})(|\mathbf{k}| - |\mathbf{q}| \cos \theta_k)} \\ &\times \frac{1}{4} \sum_{m_{s_1'}, m_{s_1}, m_V, \lambda} \\ &\times |\langle \mathbf{k} m_V, \mathbf{t} m_{s_1}' | t_{VN, \gamma N}(\omega) | \mathbf{q} \lambda, \mathbf{0} m_{s_1} \rangle|^2 \\ &\times |A_T [F_T(t) + F_T^{\text{FSI}}(t')]|^2, \end{aligned} \quad (52)$$

where $t = (q - k)^2$ and $t' = (k' - k)^2$. A_T is the number of nucleons in the target nucleus T and

$$\begin{aligned} F_T^{\text{FSI}}(t') &= \int d\mathbf{k}' \langle \mathbf{k} \mathbf{P}' | T_{VA}(E) | \mathbf{k}' \bar{\mathbf{P}} \rangle \\ &\times \frac{1}{E - E_V(k') - E_A(\bar{\mathbf{P}}) + i\epsilon} F_T(t'), \end{aligned} \quad (53)$$

with $\bar{\mathbf{P}} = \mathbf{q} - \mathbf{k}'$ and $\mathbf{P}' = \mathbf{q} - \mathbf{k}$. The form factor $F_T(t)$ in Eq. (52) and (53) is calculated from [52]

$$F_T(t) = \langle \Psi_T | \sum_{i=1, A} e^{i\boldsymbol{\kappa} \cdot \mathbf{r}_i} | \Psi_T \rangle, \quad (54)$$

where $|\Psi_T\rangle$, normalized as $\langle \Psi_T | \Psi_T \rangle = 1$, is the nuclear ground state. $\boldsymbol{\kappa}$ is the three-momentum transfer to the nucleus in the rest frame of the nucleus and is related to t by

$$-t = \boldsymbol{\kappa}^2 - \omega^2, \quad (55)$$

with

$$\omega = \sqrt{\boldsymbol{\kappa}^2 + m_T^2} - m_T, \quad (56)$$

where m_T is the mass of the target nucleus T . Clearly, $F_T(t)$ is related to the nuclear charge form factor $F_c(q^2)$ (with no exchange current contribution) by

$$F_c(q^2) = F_N(q^2) F_T(q^2 = t), \quad (57)$$

where $F_N(q^2)$ is the nucleon charge form factor.

The above formulae are the same as those employed in Ref. [26] to investigate the ϕ photo-production on ${}^4\text{He}$. In this work, the nuclear form factors are calculated from the wave function generated from the Variational Monte Carlo (VMC) calculations [52] for ${}^4\text{He}$, ${}^{16}\text{O}$, and ${}^{40}\text{Ca}$. The predicted total cross sections are compared with that from the proton target in Fig. 15. At higher energies, the total cross sections are larger when heavier nuclei targets

are used as displayed in Fig. 15(a). Meanwhile, the total cross sections near the threshold are more dramatic as seen in Fig. 15(b). They are very small compared with that from the proton target (solid curve). This is not surprising, because near the threshold the cross sections are mainly from large $-t$ region where the nuclear form factors are small, as seen clearly in the top panels of Fig. 16 where the predicted differential cross sections are also presented. Here we compare the results of T^{FSI} and $T^{\text{IMP}} + T^{\text{FSI}}$. We find that the FSI effects are significant near the threshold but are very weak at rather higher energies. The measurements for heavier nuclei targets near the threshold will be very challenging and help shed light on the relevant reaction mechanism.

VI. SUMMARY AND FUTURE DEVELOPMENTS

We have used the Pom-CQM model [1, 11] for the $\gamma p \rightarrow J/\psi p$ reaction to predict the cross sections of the exclusive J/ψ photo-production on nuclei. The calculations have been performed within the multiple scattering theory by including the impulse amplitude $T_{J/\psi A, \gamma A}^{\text{IMP}}$ and the final J/ψ -nucleus scattering amplitude $T_{J/\psi A, \gamma A}^{\text{FSI}}$. The impulse term $T_{J/\psi A, \gamma A}^{\text{IMP}}$ for the deuteron target can be calculated exactly using the wave function generated from the realistic NN potentials. We have shown that, near the threshold region, the J/ψ photo-production cross sections depend strongly on the d -state of the deuteron wave function. We also find that the conventional FSA, which expresses the amplitude $T_{J/\psi A, \gamma A}^{\text{IMP}}$ in terms of the averaged $\gamma p \rightarrow J/\psi p$ amplitude and the nuclear form factor, is not valid near the threshold region but is a good approximation at higher energies.

The FSA is then applied to predict the cross sections of the J/ψ photo-production on the ${}^4\text{He}$, ${}^{16}\text{O}$, and ${}^{40}\text{Ca}$ targets using their nuclear form factors from the variational Monte-Carlo calculations of Ref. [52].

The J/ψ -nucleus scattering amplitude, which is needed to evaluate the FSI amplitude $T_{J/\psi A, \gamma A}^{\text{FSI}}$, is calculated using the first-order optical potentials which are constructed using the nuclear form factor and the J/ψ - N scattering amplitude generated from the employed Pom-CQM model. It is found that the FSI effects are significant at large $-t$ region.

The Pom-CQM model used in this work is based on the phenomenological quark- N potentials $v_{cN}(r)$ determined by fitting to the JLab data. To interpret our results in terms of the role of gluons in nuclei, it is necessary to relate $v_{cN}(r)$ to the gluons associated with the nucleon. If we also use the CQM model for nucleon, $v_{cN}(r)$ can be derived by folding a quark-quark interaction potential due to the gluon-exchange mechanisms into the constituent quark density of the nucleon. If we use the partonic model for the nucleon, a possibility is to relate $v_{cN}(r)$ to the GPD-based model of J/ψ photo-

production model of Ref. [9]. Either one is non-trivial but must be pursued in the future.

Our predictions for $A > 2$ nuclei near the threshold have been done only using the FSA, and thus are not reliable in the sub-threshold region where the bound nuclei with hidden charms [53–56] or J/ψ -nucleus resonances, if exist, can be identified. To make progress in this direction, it is necessary to go beyond the FSA and perform the calculation using the nuclear many-body wave function.

APPENDIX

The formulation of the Pom-CQM model was given in detail in Refs. [1, 11]. Here we only give the formulae which are used for the calculations in this work and are needed to develop the formulation for the J/ψ photo-production on nuclei.

In the c.m. frame, the matrix element of $T_{VN, \gamma N}^D$ of Eq. (3) can be decomposed into

$$\begin{aligned} & \langle \mathbf{p}', m_V m_{s'} | T_{VN, \gamma N}^D(W) | \mathbf{q}, \lambda m_s \rangle \\ &= \langle \mathbf{p}', m_V m_{s'} | B_{VN, \gamma N}(W) | \mathbf{q}, \lambda m_s \rangle \\ &+ \langle \mathbf{p}', m_V m_{s'} | T_{VN, \gamma N}^{\text{FSI}}(W) | \mathbf{q}, \lambda m_s \rangle, \end{aligned} \quad (58)$$

where W is the invariant mass in the initial γ - N system. The Born term illustrated in Fig. 1 can be expressed as

$$\begin{aligned} & \langle \mathbf{p}', m_V m_{s'} | B_{VN, \gamma N}(W) | \mathbf{q}, \lambda m_s \rangle \\ &= C_{\lambda, m_V} \delta_{m_s, m_{s'}} B(\mathbf{p}', \mathbf{q}, W) [2v_{cN}^B(\mathbf{q} - \mathbf{p}')], \end{aligned} \quad (59)$$

with

$$C_{\lambda, m_V} = \sum_{m_c, m_{\bar{c}}} \langle J_V m_V | \frac{1}{2} m_c m_{\bar{c}} \rangle \langle m_{\bar{c}} | \sigma \cdot \epsilon_\lambda | m_c \rangle, \quad (60)$$

and

$$v_{cN}^B(\mathbf{q} - \mathbf{p}') = \frac{1}{(2\pi)^3} \int d\mathbf{r} e^{i(\mathbf{q} - \mathbf{p}') \cdot \mathbf{r}} v_{cN}^B(r). \quad (61)$$

We note here that, for a Yukawa form of Eq. (6) for $v_{cN}^B(r)$, Eq. (61) leads to

$$\begin{aligned} & v_{cN}^B(\mathbf{q} - \mathbf{p}') \\ &= \frac{\alpha}{(2\pi)^2} \left[\frac{1}{(\mathbf{q} - \mathbf{p}')^2 + \mu_B^2} - \frac{1}{(\mathbf{q} - \mathbf{p}')^2 + \mu_B'^2} \right]. \end{aligned} \quad (62)$$

The term $B(\mathbf{p}', \mathbf{q}, W)$ in Eq. (59) involves a loop-integration over the J/ψ wave function $\phi(k)$ and is of the following form

$$\begin{aligned} B(\mathbf{p}', \mathbf{q}, W) &= \frac{1}{(2\pi)^3} \frac{e_c}{\sqrt{2|\mathbf{q}|}} \int d\mathbf{k} \phi(\mathbf{k} - \frac{1}{2}\mathbf{p}') \\ &\times \frac{1}{W - E_N(\mathbf{q}) - E_c(\mathbf{q} - \mathbf{k}) - E_c(\mathbf{k}) + i\epsilon} \\ &\times \sqrt{\frac{E_c(\mathbf{k}) + m_c}{2E_c(\mathbf{k})}} \sqrt{\frac{E_c(\mathbf{q} - \mathbf{k}) + m_c}{2E_c(\mathbf{q} - \mathbf{k})}} \\ &\times \left\{ 1 - \frac{\mathbf{k} \cdot (\mathbf{q} - \mathbf{k})}{[E_c(\mathbf{k}) + m_c][E_c(\mathbf{q} - \mathbf{k}) + m_c]} \right\}, \end{aligned} \quad (63)$$

where m_c is the constituent quark mass of charm quark c , $E_a(\mathbf{p}) = \sqrt{m_a^2 + \mathbf{p}^2}$ the energy for the particle a with mass m_a , and $e_c = \frac{2}{3}e$ with e being the electron charge.

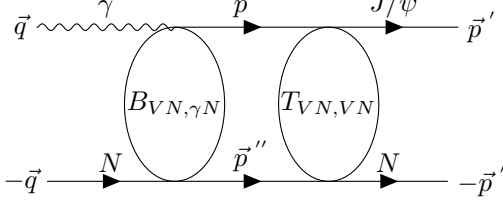


FIG. 17. J/ψ photo-production on the nucleon with the FSI effects.

The FSI term in Eq. (58) is illustrated in Fig. 17 and is of the form

$$\begin{aligned} & \langle \mathbf{p}', m_V m_{s'} | T_{VN, \gamma N}^{\text{FSI}}(W) | \mathbf{q}, \lambda m_s \rangle \\ &= \sum_{m'_V, m''_s} \int d\mathbf{p}'' \langle \mathbf{p}', m_V m_{s'} | T_{VN, VN}(W) | \mathbf{p}'', m'_V m''_s \rangle \\ & \times \frac{1}{W - E_V(p'') - E_N(p'') + i\epsilon} \\ & \times \langle \mathbf{p}'', m'_V m''_s | B_{VN, \gamma N}(W) | \mathbf{q}, \lambda m_s \rangle. \end{aligned} \quad (64)$$

With the spin independent quark- N potential defined by Eq. (7), the $J/\psi N \rightarrow J/\psi N$ scattering amplitude in the above equation can be written as

$$\begin{aligned} & \langle \mathbf{p}', m'_V m'_s | T_{VN, VN}(W) | \mathbf{p}, m_V m_s \rangle \\ &= \delta_{m_V, m'_V} \delta_{m_s, m'_s} \langle \mathbf{p}' | T_{VN}(W) | \mathbf{p} \rangle, \end{aligned} \quad (65)$$

where $\langle \mathbf{p}' | T_{VN}(W) | \mathbf{p} \rangle$ is defined by the following Lippmann-Schwinger equation

$$\begin{aligned} & \langle \mathbf{p}' | T_{VN}(W) | \mathbf{p} \rangle = \langle \mathbf{p}' | V_{VN} | \mathbf{p} \rangle \\ & + \int d\mathbf{p}'' \frac{\langle \mathbf{p}' | V_{VN} | \mathbf{p}'' \rangle \langle \mathbf{p}'' | T_{VN}(W) | \mathbf{p} \rangle}{W - E_V(p'') - E_N(p'') + i\epsilon}. \end{aligned} \quad (66)$$

Here $\langle \mathbf{p}' | V_{VN} | \mathbf{p} \rangle$, illustrated in Fig. 2, is obtained by folding $v_{cN}^{\text{FSI}}(r)$ of Eq. (7) into the J/ψ wave function and is of the following form

$$\langle \mathbf{p}' | V_{VN} | \mathbf{p} \rangle = F_V(\mathbf{t}) [2v_{cN}^{\text{FSI}}(\mathbf{t})], \quad (67)$$

where $\mathbf{t} = \mathbf{p} - \mathbf{p}'$ and

$$v_{cN}^{\text{FSI}}(\mathbf{q} - \mathbf{p}') = \frac{1}{(2\pi)^3} \int d\mathbf{r} e^{i(\mathbf{q} - \mathbf{p}') \cdot \mathbf{r}} v_{cN}^{\text{FSI}}(r), \quad (68)$$

$$F_V(\mathbf{t}) = \int d\mathbf{k} \phi^*(\mathbf{k} - \frac{\mathbf{t}}{2}) \phi(\mathbf{k}). \quad (69)$$

Here $F_V(\mathbf{t})$ is the form factor of the vector meson V and $\phi(\mathbf{k})$ is the wave function of J/ψ in momentum space.

For a Yukawa form of $v_{cN}^{\text{FSI}}(r)$ of Eq. (7), Eq. (68) has the same form as Eq. (62).

Following the approach of Donnachie and Landshoff [57–60], the Pomeron-exchange amplitude $T_{VN, \gamma N}^{\text{Pom}}(W)$ in Eq. (2) is constructed within the Regge phenomenology and is of the form

$$\begin{aligned} & \langle \mathbf{k}, m_V m_{s'} | T_{VN, \gamma N}^{\text{Pom}}(W) | \mathbf{q}, \lambda m_s \rangle \\ &= \frac{1}{(2\pi)^3} \sqrt{\frac{m_N m_N}{4E_V(\mathbf{k}) E_N(\mathbf{p}') |\mathbf{q}| E_N(\mathbf{p})}} \\ & \times [\bar{u}(p', m_{s'}) \epsilon_\mu^*(k, m_V) \mathcal{M}_{\mathbb{P}}^{\mu\nu}(k, p'; q, p) \\ & \times \epsilon_\nu(q, \lambda) u(p, m_s)], \end{aligned} \quad (70)$$

where

$$\begin{aligned} \mathcal{M}_{\mathbb{P}}^{\mu\nu}(k, p'; q, p) &= i \frac{2e m_V^2}{f_V} (qg^{\mu\nu} - q^\mu \gamma^\nu) \\ & \times [2\beta_{qV} F'_V(t)] G_{\mathbb{P}}(s, t) [3\beta_{u/d} F_1(t)]. \end{aligned} \quad (71)$$

Here m_V is the vector-meson mass, the vector-meson decay constant is $f_V = 13.4$ for $V = J/\psi$, and

$$\begin{aligned} F'_V(t) &= \frac{1}{m_V^2 - t} \left(\frac{2\mu_0^2}{2\mu_0^2 + m_V^2 - t} \right), \\ F_1(t) &= \frac{4m_N^2 - 2.8t}{(4m_N^2 - t)(1 - t/0.71)^2}, \end{aligned} \quad (72)$$

where $t = (q - k)^2 = (p - p')^2$, t is in the unit of GeV^2 , and m_N is the nucleon mass. The propagator $G_{\mathbb{P}}(s, t)$ of the Pomeron in Eq. (71) follows the Regge phenomenology form

$$G_{\mathbb{P}} = \left(\frac{s}{s_0} \right)^{\alpha_{\mathbb{P}}(t) - 1} \exp \left\{ -\frac{i\pi}{2} [\alpha_{\mathbb{P}}(t) - 1] \right\}, \quad (73)$$

where $s = (q + p)^2 = W^2$, $\alpha_{\mathbb{P}}(t) = \alpha_0 + \alpha' t$, and $s_0 = 1/\alpha'_{\mathbb{P}}$. We use the value of $\alpha' = 0.25 \text{ GeV}^{-2}$ from the works of Refs. [57–60]. The amplitude $T_{VN, \gamma N}^{\text{Pom}}(W)$ has been determined in Refs. [1, 6, 48] by fitting the data of total cross sections up to $W = 300 \text{ GeV}$. The resulting parameters are $\mu_0 = 1.1 \text{ GeV}^2$, $\beta_{u/d} = 2.07 \text{ GeV}^{-1}$, $\beta_c = 0.32 \text{ GeV}^{-1}$, and $\alpha_0 = 1.25$. Thus the remaining parameters of the Pom-CQM model in investigating the JLab data are α_a , μ_a , and N_a for $a = (\text{B}, \text{FSI})$ of the quark- N potentials given in Eqs. (6)-(7).

ACKNOWLEDGMENTS

The work of S.-H.K. is supported by Basic Science Research Program through the National Research Foundation of Korea (NRF) under Grants No. 2021R1A6A1A03043957 and No. 2022R1I1A1A01054390. T.-S.H.L. and R.B.W. are supported by the Office of Science of the U.S. Department of Energy under Contract No. DE-AC02-05CH1123.

- [1] T. S. H. Lee, S. Sakinah, and Y. Oh, Models of J/ψ photo-production reactions on the nucleon, *Eur. Phys. J. A* **58**, 252 (2022).
- [2] A. Ali *et al.* (GlueX Collaboration), First measurement of near-threshold J/ψ exclusive photoproduction off the proton, *Phys. Rev. Lett.* **123**, 072001 (2019).
- [3] S. Adhikari *et al.* (GlueX Collaboration), Measurement of the J/ψ photoproduction cross section over the full near-threshold kinematic region, *Phys. Rev. C* **108**, 025201 (2023).
- [4] B. Duran *et al.*, Determining the gluonic gravitational form factors of the proton, *Nature* **615**, 813 (2023).
- [5] S. J. Brodsky, E. Chudakov, P. Hoyer, and J. M. Laget, Photoproduction of charm near threshold, *Phys. Lett. B* **498**, 23 (2001).
- [6] T. S. H. Lee, Pomeron-LQCD model of J/ψ photoproduction on the nucleon, [arXiv:2004.13934 \[nucl-th\]](https://arxiv.org/abs/2004.13934).
- [7] K. A. Mamo and I. Zahed, Diffractive photoproduction of J/ψ and Υ using holographic QCD: Gravitational form factors and GPD of gluons in the proton, *Phys. Rev. D* **101**, 086003 (2020).
- [8] M. L. Du, V. Baru, F. K. Guo, C. Hanhart, U. G. Meißner, A. Nefediev, and I. Strakovsky, Deciphering the mechanism of near-threshold J/ψ photoproduction, *Eur. Phys. J. C* **80**, 1053 (2020).
- [9] Y. Guo, X. Ji, and Y. Liu, QCD Analysis of near-threshold photon-proton production of heavy quarkonium, *Phys. Rev. D* **103**, 096010 (2021).
- [10] D. Winney *et al.* (Joint Physics Analysis Center), Dynamics in near-threshold J/ψ photoproduction, *Phys. Rev. D* **108**, 054018 (2023).
- [11] S. Sakinah, T. S. H. Lee, and H. M. Choi, Dynamical model of J/ψ photoproduction on the nucleon, *Phys. Rev. C* **109**, 065204 (2024).
- [12] L. Tang, Y. X. Yang, Z. F. Cui, and C. D. Roberts, J/ψ photoproduction: threshold to very high energy, *Phys. Lett. B* **856**, 138904 (2024).
- [13] J. Arrington *et al.*, Physics with CEBAF at 12 GeV and future opportunities, *Prog. Part. Nucl. Phys.* **127**, 103985 (2022).
- [14] A. Accardi *et al.*, Strong interaction physics at the luminosity frontier with 22 GeV electrons at Jefferson Lab, *Eur. Phys. J. A* **60**, 173 (2024).
- [15] T. Liu, Z. Zhao, M. Cai, D. Byer, and H. Gao, Sub-threshold production of J/ψ mesons from the deuteron with the proposed solenoidal large intensity device, *Phys. Rev. C* **109**, 065206 (2024).
- [16] R. Tyson, D. G. Ireland, and B. McKinnon, Near-threshold J/ψ photoproduction off the proton and neutron with CLAS12, *Nuovo Cim. C* **47**, 212 (2024).
- [17] J. R. Pybus *et al.*, First measurement of near- and sub-threshold J/ψ photoproduction off nuclei, [arXiv:2409.18463 \[nucl-ex\]](https://arxiv.org/abs/2409.18463).
- [18] A. Accardi *et al.*, Electron Ion Collider: The next QCD frontier: Understanding the glue that binds us all, *Eur. Phys. J. A* **52**, 268 (2016).
- [19] R. Abir *et al.*, The case for an EIC theory alliance: Theoretical challenges of the EIC, [arXiv:2305.14572 \[hep-ph\]](https://arxiv.org/abs/2305.14572).
- [20] X. Wang, X. Cao, A. Guo, L. Gong, X. S. Kang, Y. T. Liang, J. J. Wu, and Y. P. Xie, Exclusive charmonium production at the electron-ion collider in China, *Eur. Phys. J. C* **84**, 684 (2024).
- [21] A. K. Kerman, H. McManus, and R. M. Thaler, The scattering of fast nucleons from nuclei, *Annals Phys.* **8**, 551 (1959).
- [22] R. H. Landau, S. C. Phatak, and F. Tabakin, Improved theoretical pion-nucleus optical potentials, *Annals Phys.* **78**, 299 (1973).
- [23] T. S. H. Lee and F. Tabakin, Momentum-space study of pion-nucleus inelastic scattering, *Nucl. Phys. A* **226**, 253 (1974).
- [24] H. Feshbach, *Theoretical Nuclear Physics: Nuclear Reactions*, John Wiley and Sons, Inc., New York, 1992.
- [25] K.M. Watson, Quantum mechanical transport theory. I. Incoherent processes, *Phys. Rev.* **118**, 886 (1960).
- [26] S. H. Kim, T. S. H. Lee, S. i. Nam, and Y. Oh, Dynamical model of ϕ meson photoproduction on the nucleon and ${}^4\text{He}$, *Phys. Rev. C* **104**, 045202 (2021).
- [27] T. Hiraiwa *et al.* (LEPS Collaboration), First measurement of coherent ϕ -meson photoproduction from ${}^4\text{He}$ near threshold, *Phys. Rev. C* **97**, 035208 (2018).
- [28] Y. Hatta, M. Strikman, J. Xu, and F. Yuan, Sub-threshold J/ψ and Υ production in γA collisions, *Phys. Lett. B* **803**, 135321 (2020).
- [29] F. He and I. Zahed, Threshold photo-production of J/ψ off light nuclei, [arXiv:2407.09991 \[nucl-th\]](https://arxiv.org/abs/2407.09991).
- [30] M. L. Goldberger and K. M. Watson, *Collision Theory*, R. E. Krieger Pub. Co., Huntington, New York, 1975.
- [31] T. Sato and T. S. H. Lee, Meson exchange model for πN scattering and $\gamma N \rightarrow \pi N$ reaction, *Phys. Rev. C* **54**, 2660 (1996).
- [32] A. Matsuyama, T. Sato, and T. S. H. Lee, Dynamical coupled-channel model of meson production reactions in the nucleon resonance region, *Phys. Rept.* **439**, 193 (2007).
- [33] H. Kamano, S. X. Nakamura, T. S. H. Lee, and T. Sato, Nucleon resonances within a dynamical coupled-channels model of πN and γN reactions, *Phys. Rev. C* **88**, 035209 (2013).
- [34] J. Segovia, D. R. Entem, F. Fernandez, and E. Hernandez, Constituent quark model description of charmonium phenomenology, *Int. J. Mod. Phys. E* **22**, 1330026 (2013).
- [35] M. E. Binkley *et al.*, J/ψ photoproduction from 60 to 300 GeV/c, *Phys. Rev. Lett.* **48**, 73 (1982).
- [36] P. L. Frabetti *et al.*, A Measurement of elastic J/ψ photoproduction cross section at Fermilab E687, *Phys. Lett. B* **316**, 197 (1993).
- [37] S. Chekanov *et al.* (ZEUS Collaboration), Exclusive photoproduction of J/ψ mesons at HERA, *Eur. Phys. J. C* **24**, 345 (2002).
- [38] S. Aid *et al.* (H1 Collaboration), Elastic and inelastic photoproduction of J/ψ mesons at HERA, *Nucl. Phys. B* **472**, 3 (1996).
- [39] C. Adloff *et al.* (H1 Collaboration), Elastic photoproduction of J/ψ and Υ mesons at HERA, *Phys. Lett. B* **483**, 23 (2000).
- [40] U. Camerini, J. G. Learned, R. Prepost, C. M. Spencer, D. E. Wisner, W. Ash, R. L. Anderson, D. Ritson, D. Sherden, and C. K. Sinclair, Photoproduction of the ψ Particles, *Phys. Rev. Lett.* **35**, 483 (1975).
- [41] R. B. Wiringa, V. G. J. Stoks, and R. Schiavilla, An accurate nucleon-nucleon potential with charge indepen-

- dence breaking, *Phys. Rev. C* **51**, 38 (1995).
- [42] M. Piarulli, L. Girlanda, R. Schiavilla, A. Kievsky, A. Lovato, L. E. Marcucci, S. C. Pieper, M. Viviani, and R. B. Wiringa, Local chiral potentials with Δ -intermediate states and the structure of light nuclei, *Phys. Rev. C* **94**, 054007 (2016).
- [43] R. Machleidt, The meson theory of nuclear forces and nuclear structure, *Adv. Nucl. Phys.* **19**, 189 (1989).
- [44] H. Kamada, W. Gloeckle, J. Golak, and C. Elster, Lorentz boosted NN potential for few body systems: Application to the three nucleon bound state, *Phys. Rev. C* **66**, 044010 (2002).
- [45] H. Witala, J. Golak, W. Gloeckle, and H. Kamada, Relativistic effects in neutron-deuteron elastic scattering, *Phys. Rev. C* **71**, 054001 (2005).
- [46] H. Witala, J. Golak, R. Skibinski, W. Gloeckle, W. N. Polyzou, and H. Kamada, Relativity and the low-energy nd A_y puzzle, *Phys. Rev. C* **77**, 034004 (2008).
- [47] A. Grassi, J. Golak, W. N. Polyzou, R. Skibiński, H. Witala, and H. Kamada, Electron and neutrino scattering off the deuteron in a relativistic framework, *Phys. Rev. C* **107**, 024617 (2023).
- [48] J. J. Wu and T. S. H. Lee, Production of J/ψ on the nucleon and on deuteron targets, *Phys. Rev. C* **88**, 015205 (2013).
- [49] P. A. M. Dirac, Forms of relativistic dynamics, *Rev. Mod. Phys.* **21**, 392 (1949).
- [50] B. D. Keister and W. N. Polyzou, Relativistic Hamiltonian dynamics in nuclear and particle physics, *Adv. Nucl. Phys.* **20**, 225 (1991).
- [51] M. I. Haftel and F. Tabakin, Nuclear saturation and the smoothness of nucleon-nucleon potentials, *Nucl. Phys. A* **158**, 1 (1970).
- [52] D. Lonardoni, A. Lovato, S. C. Pieper, and R. B. Wiringa, Variational calculation of the ground state of closed-shell nuclei up to $A = 40$, *Phys. Rev. C* **96**, 024326 (2017).
- [53] S. J. Brodsky, I. A. Schmidt, and G. F. de Teramond, Nuclear-bound quarkonium, *Phys. Rev. Lett.* **64**, 1011 (1990).
- [54] H. Gao, T. S. H. Lee, and V. Marinov, ϕ - N bound state, *Phys. Rev. C* **63**, 022201 (2001).
- [55] V. B. Belyaev, N. V. Shevchenko, A. I. Fix, and W. Sandhas, Binding of charmonium with two- and three-body nuclei, *Nucl. Phys. A* **780**, 100 (2006).
- [56] J. J. Wu and T. S. H. Lee, Photo-production of bound states with hidden charms, *Phys. Rev. C* **86**, 065203 (2012).
- [57] A. Donnachie and P. V. Landshoff, Elastic scattering and diffraction dissociation, *Nucl. Phys. B* **244**, 322 (1984).
- [58] A. Donnachie and P. V. Landshoff, Total cross sections, *Phys. Lett. B* **296**, 227 (1992).
- [59] A. Donnachie and P. V. Landshoff, Exclusive vector meson production at HERA, *Phys. Lett. B* **348**, 213 (1995).
- [60] A. Donnachie and P. V. Landshoff, Small x : Two pomerons!, *Phys. Lett. B* **437**, 408 (1998).